energies

MDPI

Article

Impact of H_2 Blending of Methane on Micro-Diffusion Combustion in a Planar Micro-Combustor with Splitter

Sreejith Sudarsanan [1], Ratna Kishore Velamati [1,*], Awad B. S. Alquaity [2,3] and Prabhu Selvaraj [1,*]

[1] Department of Mechanical Engineering, Amrita School of Engineering, Amrita Vishwa Vidyapeetham, Coimbatore 641112, India; s_sreejith@cb.students.amrita.edu
[2] Department of Mechanical Engineering, King Fahd University of Petroleum & Minerals, Dhahran 31261, Saudi Arabia; awad.alquaity@kfupm.edu.sa
[3] Center for Hydrogen and Energy Storage, King Fahd University of Petroleum & Minerals, Dhahran 31261, Saudi Arabia
* Correspondence: v_ratnakishore@cb.amrita.edu (R.K.V.); s_prabhu1@cb.amrita.edu (P.S.)

Abstract: An investigation into the non-premixed combustion characteristics of methane in a planar micro-combustor with a splitter was performed. The impact of blending methane with hydrogen on these characteristics was also analyzed. Additionally, the effects of inlet velocity and global equivalence ratio on flame location, flame temperature, combustion efficiency and outer wall temperature were studied for three different fuel compositions: pure methane (MH0), 60% methane with 40% hydrogen (MH40), and 40% methane with 60% hydrogen (MH60)). A heat recirculation analysis of the combustor wall was conducted to determine the amount of heat recirculated into the unburnt gas at various inlet velocities for all three fuel compositions. The results demonstrated that the stability limit of methane in terms of inlet velocity (1–2 m/s) and global equivalence ratio (1.0–1.2) was significantly enhanced to 1–3 m/s and 0.8–1.2, respectively, with the addition of hydrogen. At an inlet velocity of 2 m/s, the flame location of 3.6 mm for MH0 was significantly improved to 2.2 mm for MH60. Additionally, outer wall temperature exhibited a rise of 100 K for MH60 compared to MH0. Furthermore, from heat recirculation analysis, when the ratio of heat recirculated to heat loss exceeded unity, the flame started exhibiting the lift-off phenomenon for all the fuel compositions.

Keywords: micro-combustion; hydrogen; diffusion; heat recirculation

Citation: Sudarsanan, S.; Velamati, R.K.; Alquaity, A.B.S.; Selvaraj, P. Impact of H_2 Blending of Methane on Micro-Diffusion Combustion in a Planar Micro-Combustor with Splitter. *Energies* **2024**, *17*, 970. https://doi.org/10.3390/en17040970

Academic Editors: Albert Ratner, Antonio Ficarella, Donato Fontanarosa and Maria Grazia De Giorgi

Received: 19 December 2023
Revised: 9 February 2024
Accepted: 12 February 2024
Published: 19 February 2024

1. Introduction

The ever-growing demand for batteries for small-scale portable electronic devices with features like larger energy density, shorter recharge time and better performance has paved the way for advanced micro-electro-mechanical systems (MEMSs) to be developed rapidly. Because conventional chemical batteries possess problems like low power density, long recharging time and environmental pollution, etc., combustion based micro-devices are one of the best alternatives because of their very high specific energy, which is several times higher than that of the most advanced chemical batteries [1]. Combustion-based micro-power devices include micro-gas turbines, micro-heaters, micro-thermo-electric generators [2], micro-thermo photo voltaic generators [3] and micro-fuel cells. Although some of the devices mentioned above are very difficult fabricate and operate, thermo-electric generators have been found to be a feasible option. This is because they can convert a certain percentage of thermal energy received from the micro-combustor into electrical energy through the Seebeck effect. The characteristic scale of micro-combustors is typically two orders of magnitude smaller than that of conventional combustors; thus, the surface to volume ratio is greatly increased, which eventually leads to the short residence time of the gaseous mixture, a significant heat loss effect, and a radical quenching effect. Flame stability in micro-combustors faces severe challenges, especially for premixed combustion.

Numerous studies have been conducted on premixed combustion with different fuels such as H_2, CH_4, C_3H_8, $NH_{3,\ etc.}$ and various geometrical configurations, both simple types (like planar [4], rectangular [5], and cylindrical) and modified types (with backward steps [6], cavities [7], and porous media [8] as well as the Swiss-roll type, swirling [9], splitter plate, convergent–divergent type, bluff body [10], catalytic type, cross plate insert [11] etc.). Cai et al. [12] numerically investigated the relevance of a bluff body as well as the exergy efficiency of a hydrogen-fueled meso-combustor. It was observed that the magnitude and uniformity of the lower wall temperature was improved, and the exergy efficiency was also considerably improved at all velocities considered. Cai et al. [13] also numerically studied the effect of a secondary fuel injection on the NOx emissions of an ammonia-fueled combustor; it was observed that the NO emissions were reduced by 28%. Singh et al. [14] performed unsteady simulations for premixed CH_4–air and H_2–air mixtures in micro-tubes to analyze flame dynamics. Lamioni et al. [15] investigated the effect of slit pattern on flame structure in perforated burners and observed distinguished shaped flames as the number of slits varied. Different boundary conditions were tried and for a specific BC, the normalized flame propagation speed was found not to depend on the type of fuel. However, a geometry modification was primarily implemented so that the flow recirculation and the mixture residence time could be increased.

Ma et al. [16] studied a novel Swiss-roll micro-combustor with two combustion chambers, in which the effect of the material on the flame's blow-off limit for CH_4–air was analyzed numerically. The study revealed that the flame could be effectively anchored due to flow re-circulation with backward steps, and CH_4 blow-off limits could be further extended owing to the better heat re-circulation in the long preheating channels. Sankar et al. [17] studied the application of different techniques for implementing liquid fuels in different types of micro-combustors for power generation. Cai et al. [18] introduced a novel micro-disc burner with an annular step by using H_2 as fuel. It was observed in the study that a smaller Re value and larger Φ are suitable for the combustor; moreover, with the increase in thermal conductivity λ, the uniformity of the outer wall temperature was also increased. Additionally, as the surface emissivity ε value decreased, parameters such as the wall temperature level, the flame temperature, and the excess enthalpy zone increased; this was primarily due to smaller loss of heat to the environment, but the thermal output power of the combustor was considerably reduced. Pan et al. [5] experimentally investigated the flammability limits of a rectangular catalytic micro-channel using a CH_4–air mixture, in which stable flames were observed with mixture velocity ranging from 0.022 to 0.072 m/s for an equivalence ratio of one (Φ = 1).

Tang et al. [11] developed a micro-planar combustor with a cross plate insert using a C_3H_8–air mixture, and they experimentally and numerically investigated its combustion characteristics. For an equivalence ratio of one (Φ = 1), a stable flame was observed with mixture velocity ranging from 0.2 to 1.2 m/s. Cai et al. [19] numerically studied the flame dynamics and stability of a CH_4–air mixture in a quartz planar micro-combustor, and it was observed that the flame was stabilized, with mixture inlet velocity ranging from 0.2 to 0.4 m/s for an equivalence ratio of one. Singh et al. [20] investigated the effect of H_2 addition on the flame dynamics of premixed methane/air mixtures in a micro-tube of length 120 mm and diameter 2 mm. A FREI was studied, and it was observed that the FREI had a non-monotonic variation with the mixture. Different diameter tubes (1, 1.5, and 2 mm) were considered in order to study the effect of diameter on the FREI, and increased FREI frequency was found for the 1 mm rather than the 2 mm dia. tube. Peng et al. [21] experimentally and numerically investigated the combustion and thermal phenomena of a H_2-C_3H_8–air mixture in a stepped cylindrical tube with partially filled porous media. The study revealed that for an equivalence ratio of one, the flame was stabilized, with mixture velocity ranging from 4 to 7 m/s. From all the above discussed studies, it can be concluded that the major drawback of premixed combustion is that its stability limits are too low, which makes it really difficult for the flame to be stabilized properly, owing to the narrow

range of inlet velocities. Another drawback of premixed combustion is the high possibility of flashback.

For non-premixed combustion, also called diffusion combustion, flame stability is mainly affected by the mixing of fuel and oxidant, which results in peculiar flame behaviors. Liu et al. [22] numerically investigated the mixing of methane and oxygen in Y-shaped meso-scale combustors with and without porous media and observed that for the case with porous media, as the mass dispersion effect was more significant, fairly good mixing could be achieved even in horizontal channels of shorter length. It was also found that the mixing phenomenon became worse when the included angle between two inlet channels decreased or the inlet velocity increased. Ning et al. [23] experimentally investigated the impact of porous media on mixture ignitability, flame stability, and flammable range for diffusion methane–air flames in Y-shaped meso-scale combustors of three different diameters (i.e., d = 4, 5 and 6 mm), wherein it was observed that the ignition distance increased with increasing inlet velocity and decreased with a decreasing channel diameter. It was also observed that with the addition of porous media, the CH_4/air mixture was able to be ignited near the splitter (owing to enhanced mixing) and the flame propagation velocity was significantly decreased. Additionally, the flame stability was greatly improved and the flammable range of the combustor was enlarged. Muraleedharan et al. [24] numerically investigated the effect of wall material and thickness on flame height and flame temperature for micro-jet flames with hydrogen as fuel. It was found that when the burner conductivity was low, flame temperature was high, whereas flame length increased with thermal conductivity.

Li et al. [4] numerically studied the effects of inlet velocity and channel height on the mixing performance, flame stability limit, and combustion efficiency of H_2 and air in a 2D planar micro-combustor with a separating plate. The results revealed that improved mixing can be obtained with a decrease in inlet velocity and channel height; moreover, for identical inlet air velocities, the combustion efficiency increases with a reduction in combustor height, which indicates improved mixing in a narrower channel. Additionally, the flame blow-out limit also exhibited a non-monotonic trend with increasing combustor height, that is, a micro-combustor with a medium height could achieve the largest blow-out limit. Xiang et al. [25] experimentally investigated the effects of total flow rate and fuel/air ratio on the propagation behaviors of diffusion flames, and noise emission was observed in flame propagation in the upstream direction under comparatively higher mixture velocities. Li et al. [26] numerically studied the flame stability of a non-premixed H_2–air mixture in a micro-combustor with a slotted bluff body and found that for a medium blockage ratio of 0.55, the flame blow-off limit appeared to be the highest (34 m/s). It was also found that as the blockage ratio increased, a stretching effect occurred, which ultimately resulted in local extinction and flame splitting. As we have discussed in premixed combustion, plenty of research has been carried out on non-premixed combustion with various geometries and different fuels as well. Among these configurations, some prominent ones include central and bilateral bluff bodies [27], a Swiss-roll combustor [16], a swirling micro-combustor [28], and a micro-disc-combustor with an annular step and radial preheated channel [29].

The key takeaway Is that non-premixed combustion is the best alternative to premixed combustion as the former can overcome the major drawbacks of the latter, which are flame stability range and flashback. Plenty of research has been conducted on non-premixed combustion with several geometrical configurations as well as various fuels, but one research area which is yet to be explored completely is that of blended fuels, which has always been an area of interest; this is because the combustion phenomenon can be enhanced in multiple ways by blending hydrocarbon fuels such as methane, propane, etc. with other components such as hydrogen. Hydrogen was chosen as the blending component owing to its high laminar burning velocity and stability range. Zhou et al. [30] studied flame shape transition and structure characteristics by adding H_2 to CH_4 to a planar micro-combustor (but for premixed combustion). The results showed immense improvement in flame blow-out limit, due to the higher laminar flame speed of hydrogen compared to methane. Balaji et al. [31]

suggested the manufacturing of hydrogen from biomass by anaerobic digestion. Another alternative is biogas dry reformation. It was observed that the process absorbs CO_2 rather than emitting it. Hydrogen was produced from CH_4, CO_2, and H_2O (at rates of 52%, 38% and 10%, respectively) at a temperature of 837.5 °C.

Hou et al. [32] studied the effect of hydrogen addition (up to 25%) for methane meso- scale combustion and observed that the combustible range is significantly enhanced. Additionally, the combustion reaction was enhanced and the blow-off limit was extended due to the improved chemical effect. Guo et al. [33] also experimentally and numerically investigated the effect of hydrogen addition to methane-air flames, and it was observed that FREI and global quenching show a monotonic decrease. It was also observed that heat loss to the combustor walls is very relevant in cases of flame stabilization, and the quenching distance of CH_4-H_2 flames decreases as more hydrogen is added. Wang et al. [34] investigated the dynamics of FREI with the addition of hydrogen to methane–air micro-combustion and observed that as the quantity of hydrogen increased, wall temperature showed a decreasing tendency while the flame propagated faster. Raissi et al. [35] explored the effect of adding hydrogen to a methane–air composition and found that it caused nonlinear changes in pressure, velocity, and temperature inside the combustor. Eckart et al. [36] investigated the extinction strain rate of CH_4-H_2 diffusion flames for a counter-flow configuration by varying the oxygen content in the oxidizer, and the results showed that as the oxygen content reduced, ESR also reduced. The research also included a comparison of reaction mechanisms and proved that along with LBV, ESR can also be an optimization criterion. Rajamanickam et al. [37] experimentally examined the effect of hydrogen addition to methane in a canonical combustor with a bluff body, and the study revealed that when methane was enriched with more than 30% hydrogen, local extinctions disappeared and vortex shredding modes were completely suppressed. Moreover, the study established the significance of adding hydrogen for the stabilization of turbulent flames. Shin et al. [38] analyzed the effect of hydrogen addition on flame structure and stability to methane, propane, and nitrogen in a coaxial diffusion combustor. The analysis disclosed thinner flame length and width. Additionally, high OH intensity and expansion of the flame stability region were observed as hydrogen was added. Wei et al. [39] experimentally investigated the combustion characteristics of a combustor with a block with premixed CH_4-H_2 blends for micro-TPV application. While attempting to enhance the performance of combustor, the dimensions of the block, CH_4 mixing ratio, and combustor length were varied; finally, the optimum performance was achieved with a combustor length of 29 mm, a block thickness 0.6 mm, and a CH_4 molar fraction of 10%. The maximum power output was 2.9 W with an efficiency of 2.2%.

Therefore, understanding the trend in flame stabilization when adding H_2 to CH_4 in different proportions as fuel is relevant in that it will contribute to the area of combustion research. So, we proposed to investigate the effect of the addition of H_2 to CH_4 by comparing different combustion parameters such as the flame location, flame temperature, combustion efficiency, etc. of pure methane to methane blended with hydrogen (40% CH_4-60% H_2 by volume). To further understand the transition of parameters, an intermediate case (60% CH_4-40% H_2) was also considered.

2. Numerical Methodology

2.1. Geometric Model

The geometric model of the planar combustor with a splitter plate is schematically shown in Figure 1. The total length (L_0) of the combustor is 16 mm with a height (H_0) of 1 mm. The inlet is separated into two equal parts by a splitter plate at the center, which has a length of 2 mm (L_1). The fuel and air inlets have a height (H_1) of 0.4 mm each, where the upper port is for fuel and the lower port is for air. The thickness of the combustor walls (W_0) and that of the splitter plate (W_1) are 0.2 mm each. The dimensions of the combustor were adopted from the work carried out by Li et al. [4].

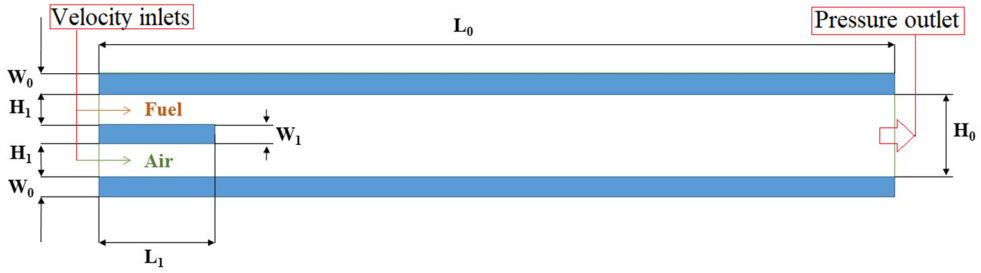

Figure 1. Schematic diagram of the micro-combustor.

2.2. Mathematical Model

Since the Knudsen number (Kn) in this work is 10^{-5}, which is much lower than the critical value of 0.001, flow shall be considered continuous and Navier–Stokes equations are applicable here. The maximum Reynolds number (Re) for the gaseous mixture was calculated to be around 170, which makes the laminar steady flow model valid for the present study. For a planar combustor, the width is assumed to be infinite, hence the numerical investigation shall be simplified into a two-dimensional approach.

Governing equations are given below.

Continuity equation:

$$\nabla . \left(\rho \vec{u} \right) = 0 \tag{1}$$

Momentum equation:

$$\rho\left(\vec{u} . \nabla \vec{u}\right) = -\nabla P + \nabla . \left(\mu \left[\nabla \vec{u} + \left(\nabla \vec{u} \right)^T - \frac{2}{3} \nabla . \vec{u} I \right] \right) \tag{2}$$

Energy equation:

$$\nabla . \vec{u} \left(\rho E_t + P \right) = \nabla . \left[k_f \nabla T - \left(\sum_j h_j \vec{J_j} \right) + \left(\mu \left[\nabla \vec{u} + \left(\nabla \vec{u} \right)^T - \frac{2}{3} \nabla . \vec{u} I \right] \right) . \vec{u} \right] + S_f \tag{3}$$

Species equation:

$$\nabla . \left(\rho \vec{u} Y_j \right) = \nabla \vec{J_j} + \omega_j \tag{4}$$

where ρ is the density of the fluid, $\vec{u}$ is the velocity component, P is the gas pressure, k_f is the thermal conductivity of the fluid, E_t is the fluid energy, and S_f is the source term. h_j and $\vec{J_j}$ are the enthalpy and diffusion flux of the *jth* species.

2.3. Computation Scheme

GRI MECH 3.0 [40] (53 species and 325 reactions) was adopted as the reaction mechanism. Fuel and oxidizer inlet ports were specified as velocity inlets with a temperature of 300 K, whereas the pressure outlets had a pressure magnitude of 1 atm. Owing to its high strength and corrosion resistance, stainless steel was chosen as the solid material for the combustor.

Heat transfer from the outer wall to surroundings was calculated using the following Equation:

$$q = h(T_w - T_\infty) + \varepsilon_w \sigma \left((T_w)^4 - (T_\infty)^4 \right) \tag{5}$$

where h denotes the natural convection heat transfer coefficient (25 W/(m^2.K); T_w, T_∞ represent the outer wall and ambient temperatures, respectively. ε_w represents the emissivity of the wall (0.6), and σ is the Stephan–Boltzman constant (5.67×10^{-8} W/(m^2.K^4)).

The continuity, momentum, energy, and species equations were solved using the computational fluid dynamics software FLUENT 2023R1 [41], based on the finite volume method (FVM). The equations were discretized using the second-order upwind scheme, and the 'SIMPLE' algorithm was used for pressure–velocity coupling. The density of the gaseous mixture was calculated based on the ideal gas law. Considering the large variations in rates of chemical reactions, a stiff chemistry solver was adopted for the improved convergence of iterations. The CFD calculation was considered to be converged when the residuals of all governing equations were less than 10^{-6}. A temperature patch of 2400 K from the mixture outlet towards the inlet was adopted to initiate the combustion reaction.

The global equivalence ratio (Φ_g) was used to specify the fuel–air ratio at the inlets. Inlet air velocity (V_{air}) is referred to as inlet velocity. As shown in Table 1, fuel compositions were specified as MH0, MH40, and MH60, which indicates pure methane (100% methane), 60% methane with 40% hydrogen, and 40% methane with 60% hydrogen, respectively.

Table 1. Designation of fuel compositions based on the percentage of components by volume.

Sl. No.	Designation	CH_4 (%)	H_2 (%)
1	MH0	100	0
2	MH40	60	40
3	MH60	40	60

Combustion efficiency (η_c) is calculated as the ratio of heat energy released by fuel during the combustion process to the input heat energy possessed by fuel.

In the case of pure methane, the major combustible elements in exhaust gas being CH_4 and CO, η_c is calculated as follows:

$$\eta_c = 1 - \frac{m_{out,\ CH4}.\ \Delta h_{CH4} + m_{out,\ CO}.\ \Delta h_{CO}}{m_{in,\ CH4}.\ \Delta h_{CH4}} \tag{6}$$

For hydrogen-blended methane, the major combustible elements become CH_4, H_2, and CO, and therefore η_c is calculated by using the modified equation given below.

$$\eta_c = 1 - \frac{m_{out,\ CH4}.\ \Delta h_{CH4} + m_{out,\ H2}.\ \Delta h_{H2} + m_{out,\ CO}.\ \Delta h_{CO}}{m_{in,\ CH4}.\ \Delta h_{CH4} + m_{in,\ H2}.\ \Delta h_{H2}} \tag{7}$$

where $m_{out,\,CH4}$, $m_{out,\,H2}$, and $m_{out,\,CO}$ are the mass flow rates of CH_4, H_2, and CO at the combustor outlet, respectively. Δh_{CH4}, Δh_{H2}, and Δh_{CO} are the reaction enthalpies of CH_4, H_2, and CO, respectively. $m_{in,\,CH4}$ and $m_{in,\,H2}$ represent the mass flow rates of CH_4 and H_2 at the inlet.

Combustor efficiency (η_{cr}) is defined as the ratio of the heat released during combustion to the heat input:

$$\eta_{cr} = \frac{\left(\dot{m}_{out} \times C_p \times \Delta T\right) - \left[\left(\dot{m}_{in,air} \times C_p \times \Delta T\right) + \left(\dot{m}_{in,fuel} \times C_p \times \Delta T\right)\right]}{\dot{m}_{in,fuel} \times CV} \tag{8}$$

where $\dot{m}_{out}$, $\dot{m}_{in,air}$, and $\dot{m}_{in,fuel}$ are the mass flow rates of flue gas at the outlet, mass flow rate of air, and mass flow rate of fuel, respectively. C_p, ΔT, and CV are the specific heat at constant pressure, change in temperature, and calorific value of the respective components.

2.4. Grid Independence Study

The computational domain was divided into structured grids. Grid independence was verified by comparing the temperature contours and center line temperature profiles obtained using three different grid systems ($\Delta x = \Delta y$ = 0.025 mm, $\Delta x = \Delta y$ = 0.0125 and $\Delta x = \Delta y$ = 0.00625) for pure methane (MH0) with V_{air} = 1 m/s, V_{fuel} = 0.1 m/s, and ϕ_g = 1. The differences in the acquired results [Figure 2(i,ii)] were found to be negligible. Hence, in order to reduce the computational effort, a grid size of $\Delta x = \Delta y$ = 0.025 mm was adopted for final computation.

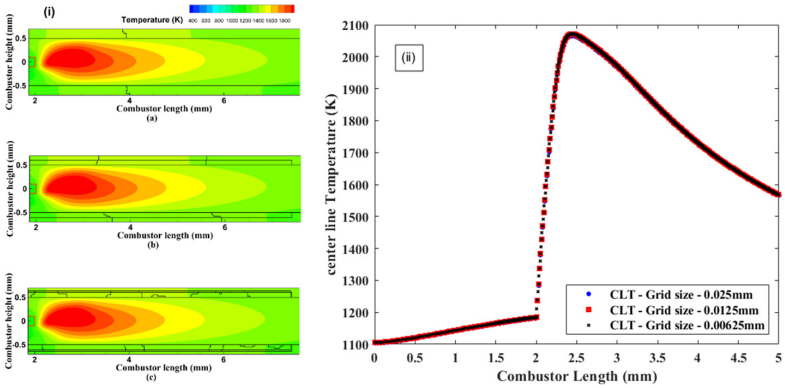

Figure 2. Grid independence study of pure methane (MH0) with V_{air} = 1 m/s and V_{fuel} = 0.1 m/s. Comparison of (**i**) temperature contours and (**ii**) center line temperature with the following grid sizes: (**a**) $\Delta x = \Delta y$ = 0.025 mm; (**b**) $\Delta x = \Delta y$ = 0.0125 mm (**c**) $\Delta x = \Delta y$ = 0.00625 mm.

2.5. Validation

Jiaqiang et al. [42] numerically investigated the characteristics of a diffusion-type micro-combustor, and the results were compared to those obtained from experiments on the mass flow rates of hydrogen and air (1.347×10^7 kg/s and 4.632×10^6 kg/s, respectively) at an equivalent ratio of unity. The same methodology was adopted and these simulations were performed in the present paper. Figure 3 shows the comparison of all the three results, from which the difference between experimental and present simulation results was observed to be less than 1.6%. The error that occurred is experimental and due to accuracy of measurement. So, it is validated that the present numerical methodology is able to deliver results that are very close to those obtained from experiments.

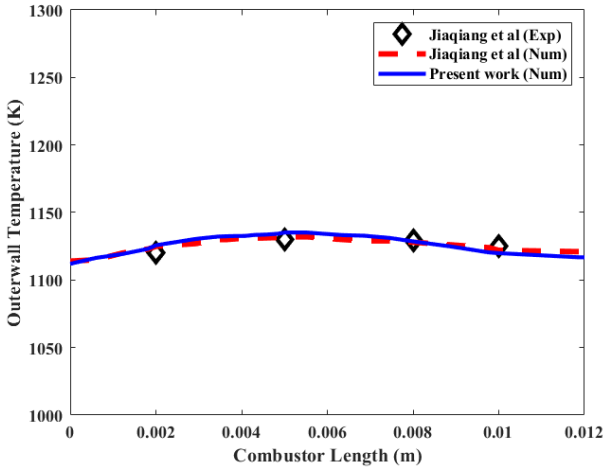

Figure 3. Validation of a diffusion-type hydrogen-fueled micro-combustor; comparison of outer wall temperature: ◆ Jiaqiang et al. (2017) [42] (Exp), ▬ ▬ Jiaqiang et al. (2017) [42] (Num) and ▬ the present work (Num).

3. Results and Discussion

3.1. Effect of Inlet Velocity and Composition on Flame Structure

This section deals with variations in flame stabilization parameters such as flame location, flame temperature, wall temperature, etc. for pure methane and hydrogen-blended methane fuels as the inlet velocity varies. Firstly, the same parameters are studied for pure methane.

3.1.1. Pure Methane

To investigate the impact of inlet velocity, steady-state numerical simulations were conducted using pure methane as fuel, maintaining a unified global equivalence ratio (i.e., a stoichiometric air–fuel ratio). Even though simulations were attempted for higher velocities, the solutions converged for velocities of air of 1, 1.5 and 2 m/s, due to methane's limited stability range. At velocities exceeding 2.5 m/s, flames were observed to be extinguished.

The flame structure of MH0 was studied by plotting the heat release contours along with temperature for inlet velocities 1 m/s, 1.5 m/s, and 2 m/s (Figure 4). From Figure 4, its evident that at lower velocity (i.e., V_{air} = 1 m/s), fuel and air were mixed at the end of the splitter and then ignited. However, the amount of fuel and air being mixed was very low, which resulted in a relatively small flame zone. The maximum flame temperature was observed to be 1900 K, and the combustor walls were heated to about 1400 K downstream of the flame. The flame was positioned slightly towards the air inlet side due to the high velocity of inlet air compared to that of methane. When the inlet air velocity was increased to 1.5 m/s, the flame was found to be lifted off the splitter and the flame thickness increased due to the increased amount of fuel and air being mixed. Upon further increasing the velocity to 2 m/s, the flame was stabilized downstream, and the flame zone extended up to the upper wall due to the presence of a rich mixture.

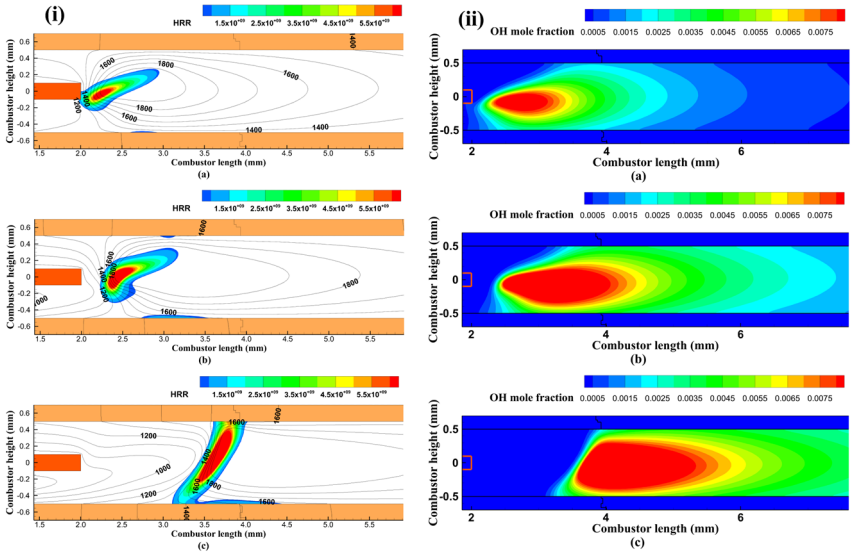

Figure 4. (**i**) Heat release rate and temperature profile and (**ii**) OH mole fraction of MH0: (**a**) V_{air} = 1 m/s; (**b**) V_{air} = 1.5 m/s; (**c**) V_{air} = 2 m/s.

Figure 4(ii) demonstrates the variation in the reaction zone for MHO, as the inlet velocity varied, from the OH mole fraction contours. At an inlet velocity of 1 m/s, the reaction zone moved slightly towards the bottom wall of the combustor due to the higher velocity of air compared to that of methane. As the inlet velocity increased to 1.5 m/s, enhanced mixing of fuel and air resulted in increased combustion, expanding the reaction zone and shifting it downstream. Further increasing the velocity to 2 m/s intensified mixing and combustion, significantly enlarging the reaction zone to almost reach both the upper and lower walls.

Figure 5(i) illustrates the temperature distribution of MH0 for inlet velocities of 1 m/s, 1.5 m/s, and 2 m/s. At 1 m/s inlet velocity, due to a weaker flame, the walls were not heated much, as shown in Figure 5(i)a; however, as the velocity increased, the flame became stronger and the walls were subsequently heated better. The flame temperature was considered to be the maximum temperature obtained at the geometric center line of the combustor. Observations indicated a clear rise in the maximum flame temperature as the inlet velocity increased, which is vividly demonstrated in Figure 5(iii). As the velocity increased, flame temperature increased from 2000 K to 2200 K. At a velocity of 2 m/s, a sudden spike in the center line temperature profile was evident (at a distance of 2 mm) due to localized heating at the splitter's tip, followed by a trend similar to that of other cases.

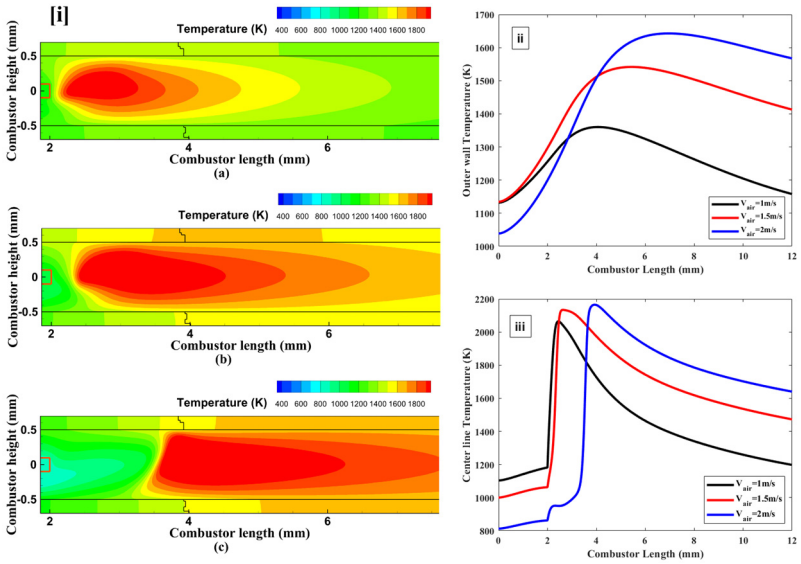

Figure 5. (**i**) Temperature contours (**ii**); outer wall temperature; and (iii) center line temperature of MH0: (**a**)V_{air} = 1 m/s; (**b**) V_{air} = 1.5 m/s; (**c**) V_{air} = 2 m/s.

The variation in the outer wall temperature also exhibited a consistent change concerning the inlet velocity, as detailed in Figure 5(ii). At an inlet velocity of 1 m/s, the maximum outer wall temperature was found to slightly exceed 1300 K at a location about 4 mm downstream of the combustor inlet. When the inlet velocity was increased to 1.5 m/s, the maximum wall temperature increased to about 1500 K. Further elevation of the velocity to 2 m/s led to an increase in the maximum wall temperature to over 1600 K positioned roughly 6 mm downstream from the combustor inlet.

3.1.2. Comparison of Pure Methane with Hydrogen-Blended Methane

Having discussed the various aspects of the combustion of MH0 in the previous section, mainly its low stability range (1–2 m/s), the same combustion characteristics for methane–hydrogen blends (MH40 and MH60) are analyzed, and the results are compared with those obtained for MH0 in this section. Hydrogen was chosen as the blending element as it is expected to increase the stability range of fuel because it possesses high laminar burning velocity and a large stability range. Thus, different combustion parameters are compared for MH0 and MH60. Additionally, the composition of MH40 was taken as an intermediate case, from which the transition in parameters can be vividly explained.

As the inlet velocity increased from 1 m/s with intervals of 0.5 m/s up to 3 m/s, the flame was able to be stabilized inside the combustor. Figure 6 depicts variation in the flame's location with respect to inlet velocity (1 m/s–3 m/s) for MH0, MH40, and MH60. The location of the flame is defined by the position of the maximum heat of the reaction from the combustor inlet along its center line. It is obvious that the value of the flame's location reduced, i.e., the lift-off tendency reduced, as the amount of hydrogen in the fuel

increased. This is because as more hydrogen was added into the fuel, its laminar burning velocity increased, and consequently, the flame moved upstream.

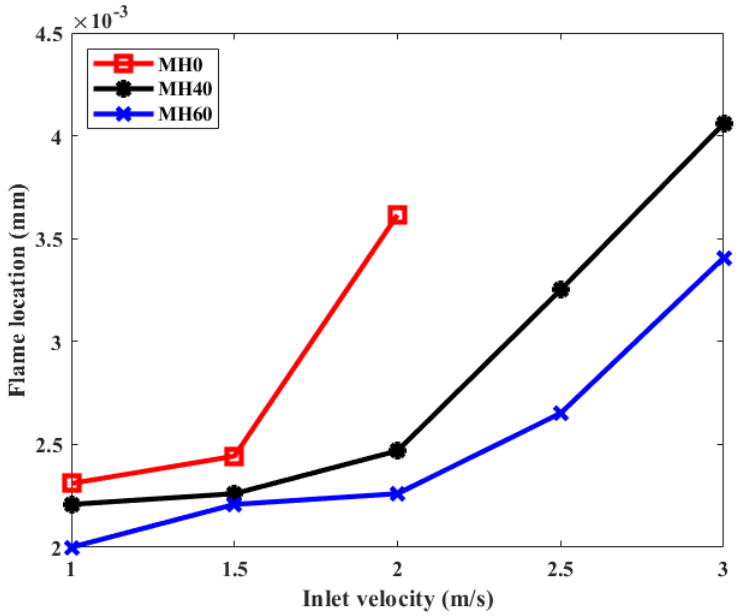

Figure 6. Variation in flame location at different inlet velocities for different fuel compositions (MH0, MH40 and MH60).

Figure 7 depicts the comparison of the flame structure and temperature profile of (i) MH0 ((a) V_{air} = 1 m/s; (b) V_{air} = 2 m/s) and MH60 ((a) V_{air} = 1 m/s; (b) V_{air} = 2 m/s; (c) V_{air} = 3 m/s) at various inlet velocities. Since the laminar burning velocity increases with the presence of hydrogen in MH60, the flame is very well attached to the tip of the splitter until the velocity reaches 2 m/s. Additionally, for MH60, when the velocity reaches 3 m/s, flame is lifted off and the flame thickness and location are almost similar to those of MH0 at a velocity of 2 m/s. So, the stability range was increased by the addition of hydrogen from 1–2 m/s for MH0 to 1–3 m/s for MH60. Figure 8 demonstrates the comparison of the reaction zone of MH0 and MH60 from the OH mole fraction distribution at different inlet velocities: (i) MH0 ((a) V_{air} = 1 m/s; (b) V_{air} = 2 m/s) and MH60 ((a) V_{air} = 1 m/s; (b) V_{air} = 2 m/s; (c) V_{air} = 3 m/s). The size of reaction zone is larger for MH60 at an inlet velocity of 1 m/s (Figure 8(ii)a) compared to that of MH0 at a velocity of 1 m/s (Figure 8(i)a). So, it is evident that the combustion reaction was enhanced by the addition of hydrogen. Additionally, the reaction zone at all velocities displayed a tendency to stay near the lower wall of the combustor wall due to the higher velocity of air enhancing the mixing process near the lower wall. At 3 m/s for MH60, the shape of the reaction zone changed, becoming similar to that of MH0 at 2 m/s. This shows that the flame was on the verge of blow-out.

The temperature distribution of MH0 and MH60 at different inlet velocities ((i) MH0 ((a) V_{air} = 1 m/s; (b) V_{air} = 2 m/s) and MH60 ((a) V_{air} = 1 m/s; (b) V_{air} = 2 m/s; (c) V_{air} = 3 m/s)) is illustrated in Figure 9. The fuel composition of MH60 shows better temperature distribution at 2 m/s, as the walls are heated to a higher and more uniform temperature. Figure 10 shows the variation in outer wall temperature and center line temperature of both the fuel compositions at different inlet velocities: (i) MH0 ((a) V_{air} = 1 m/s; (b) V_{air} = 2 m/s) and MH60 ((a) V_{air} = 1 m/s; (b) V_{air} = 2 m/s; (c) V_{air} = 3 m/s)}. The maximum outer wall temperature considerably increased from 1600 K for MH0 at an inlet velocity of 2 m/s to about 1800 K at 2.5 m/s for MH60, which is shown in Figure 10. For MH60, the maximum outer wall temperature displayed a monotonic increase until an inlet velocity of 2.5 m/s.

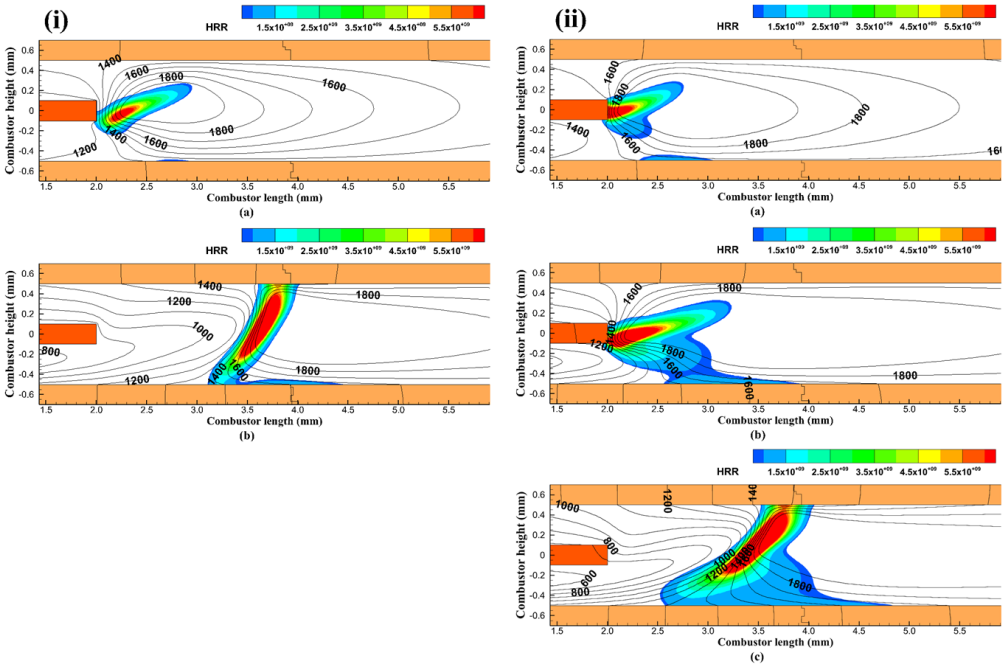

Figure 7. Comparison of the heat release rate and temperature profile of (**i**) MH0 ((**a**) V_{air} = 1 m/s; (**b**) V_{air} = 2 m/s) and (**ii**) MH60 ((**a**) V_{air} = 1 m/s; (**b**) V_{air} = 2 m/s; (**c**) V_{air} = 3 m/s).

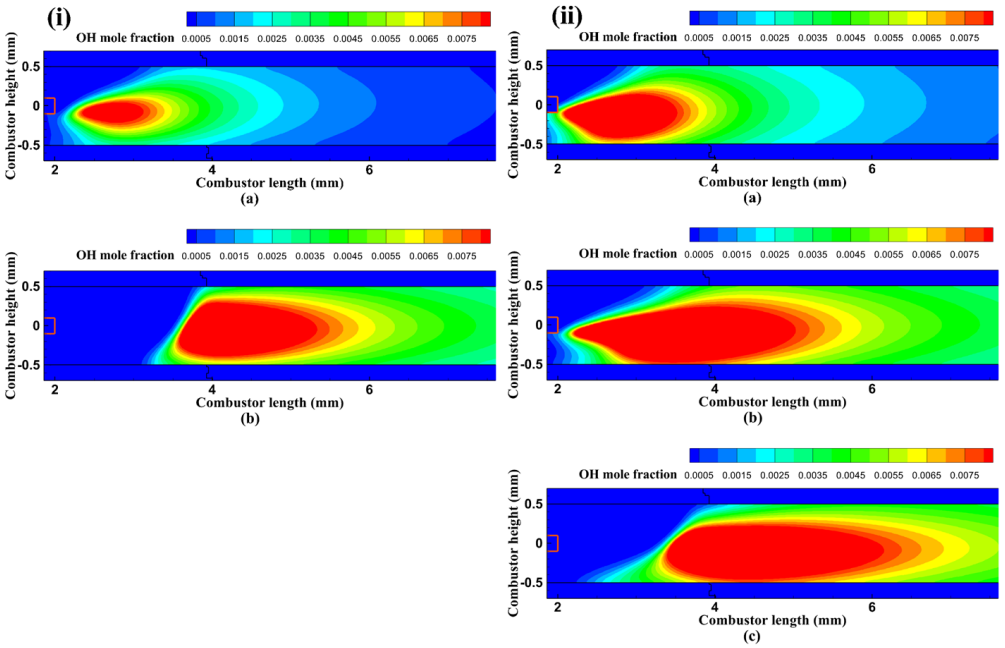

Figure 8. Comparison of the OH mole fraction of (**i**) MH0 ((**a**) V_{air} = 1 m/s; (**b**) V_{air} = 2 m/s) and (**ii**) MH60 ((**a**) V_{air} = 1 m/s; (**b**) V_{air} = 2 m/s; (**c**) V_{air} = 3 m/s).

In order to analyze the effect of fuel composition, the four distinct parameters of flame location, flame temperature, combustion efficiency, and outer wall temperature were plotted for three different fuel compositions—MH0, MH40 and MH60—at an air inlet velocity of 2 m/s, as depicted in Figure 11. Flame location, which is the distance from combustor inlet to the location of the maximum heat of reaction along the combustor's central axis, was found to be reduced from 3.6 mm to 2.3 mm as more hydrogen was added. Flame temperature, which is the maximum temperature measured along the combustor's central

axis as well as the combustion efficiency, remained almost same for all fuel compositions. The outer wall temperature showed a significant increase of about 100 K for MH60. Hence, it can be perceived that the more hydrogen that was added to methane, the more the overall combustion performance was improved; in the present study, the composition of MH60 was the most optimal among all three compositions.

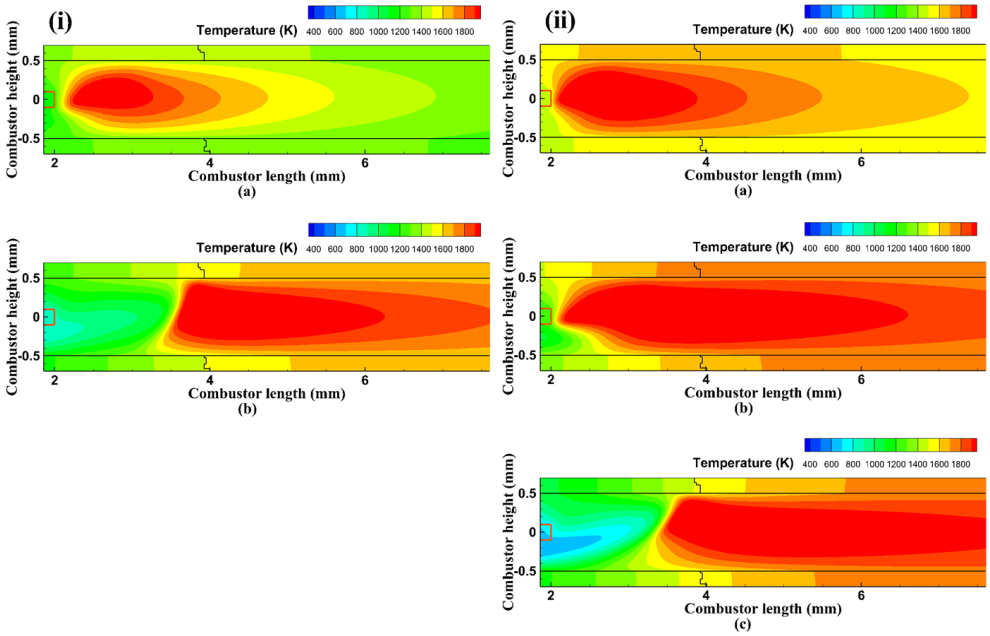

Figure 9. Comparison of the temperature distribution of (**i**) MH0 ((**a**) V_{air} = 1 m/s; (**b**) V_{air} = 2 m/s) and (**ii**) MH60 ((**a**) V_{air} = 1 m/s; (**b**) V_{air} = 2 m/s; (**c**) V_{air} = 3 m/s).

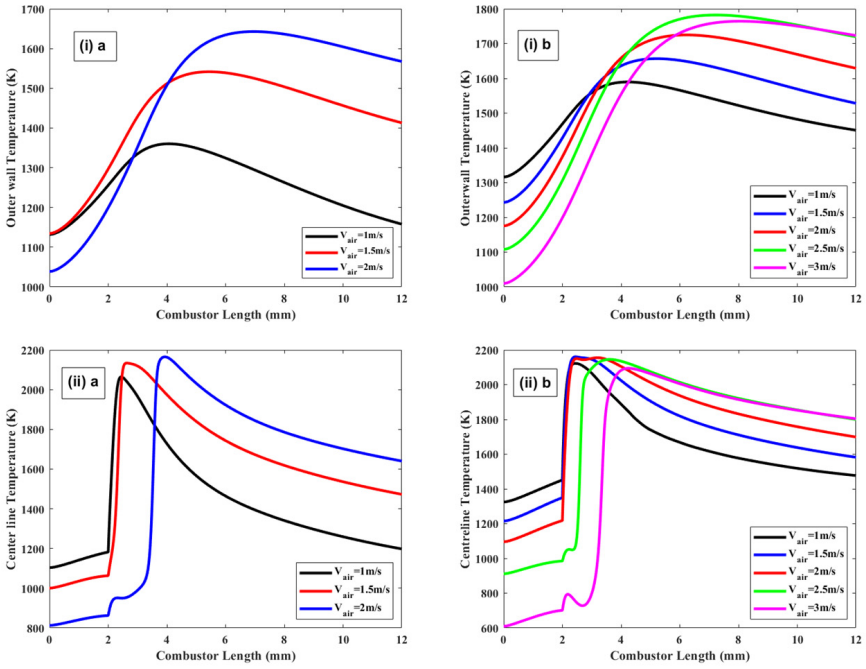

Figure 10. Comparison of variation in the (**i**) outer wall temperature (**a**) MH0 (1 m/s, 1.5 m/s and 2 m/s) and (**b**) MH60 (1 m/s, 1.5 m/s, 2 m/s, 2.5 m/s and 3 m/s) and (**ii**) center line temperature profiles of (**a**) MH0 (1 m/s, 1.5 m/s and 2 m/s) and (**b**) MH60 (1 m/s, 1.5 m/s, 2 m/s, 2.5 m/s and 3 m/s) at different inlet velocities.

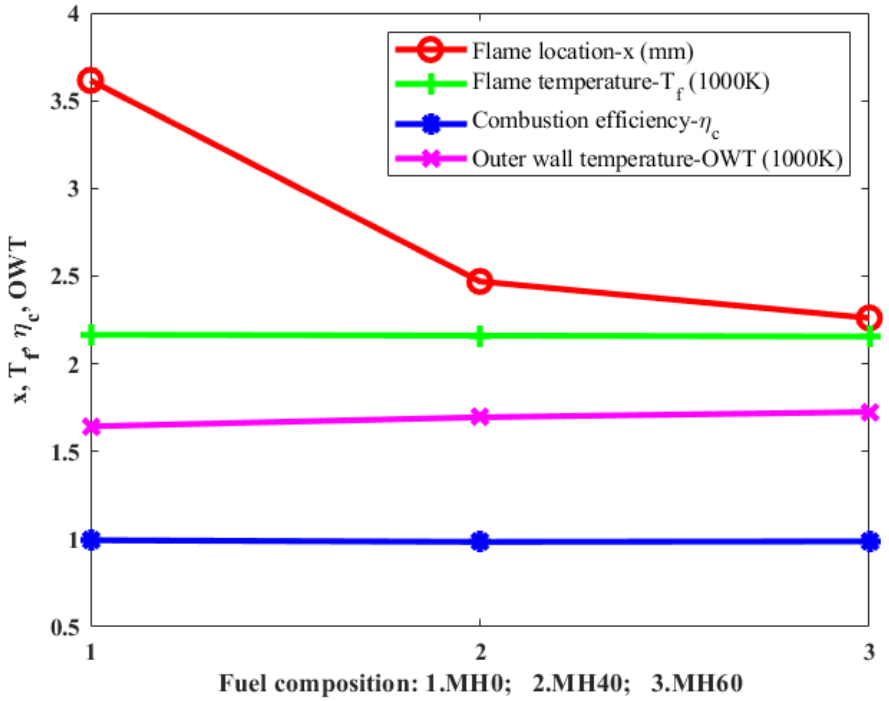

Figure 11. Variation in flame location, flame temperature, combustion efficiency, and outer wall temperature for different fuel compositions at an inlet velocity of 2 m/s.

3.2. Effect of Equivalence Ratio

The global equivalence ratio (Φ_g) refers to the ratio of the fuel flow rate to the air flow rate at the inlet.

$\Phi_g = \frac{\left(\frac{A}{F}\right)_{stoich}}{\left(\frac{A}{F}\right)_{actual}}$, where $\left(\frac{A}{F}\right)$stoich is the stoichiometric air–fuel ratio and $\left(\frac{A}{F}\right)$actual is the actual air–fuel ratio.

This term was introduced due to the nature of diffusion combustion, where the air–fuel ratio varies spatially. The variation in different combustion parameters such as flame location, flame temperature, combustion efficiency, etc. (with respect to the change in the global equivalence ratio from 0.8 to 1.2) for each composition are discussed in this section. The required global equivalence ratios can be achieved either by varying inlet fuel velocity and keeping inlet air velocity constant or by varying inlet air velocity and keeping inlet fuel velocity constant. To understand the difference between both, simulations were initially performed by varying inlet fuel velocity and keeping the air velocity constant (2 m/s). The results of the variation in flame location and flame temperature are shown in Figure 12. The flame location and temperature decreased as the amount of hydrogen increased. Moreover, from stoichiometric to rich conditions, for each fuel composition, flame location and flame height showed an increasing trend. The highest flame temperature was observed as 2280 K, when Φ_g = 1.2. Flame location showed significant improvement from 3.6 mm (MH0) to 2.2 mm (MH60) at Φ_g = 1.0.

The same simulations were repeated (keeping the inlet fuel velocity constant (0.1 m/s)) for all fuel compositions, and the inlet air velocity was varied to achieve the desired lean and rich equivalence ratios, thereby ensuring that the firing rate did not vary much, which eventually made the results comparable across all compositions at all equivalence ratios. Flame stabilization of MH0 and MH40 was found to be limited, as they exhibited stable flames for global equivalence ratios of 1 and 1.2 (i.e., stoichiometric and rich conditions) only. However, for MH60, the lean stability limit was observed to be considerably improved as the flame was stabilized in leaner conditions (Φ_g = 0.8).

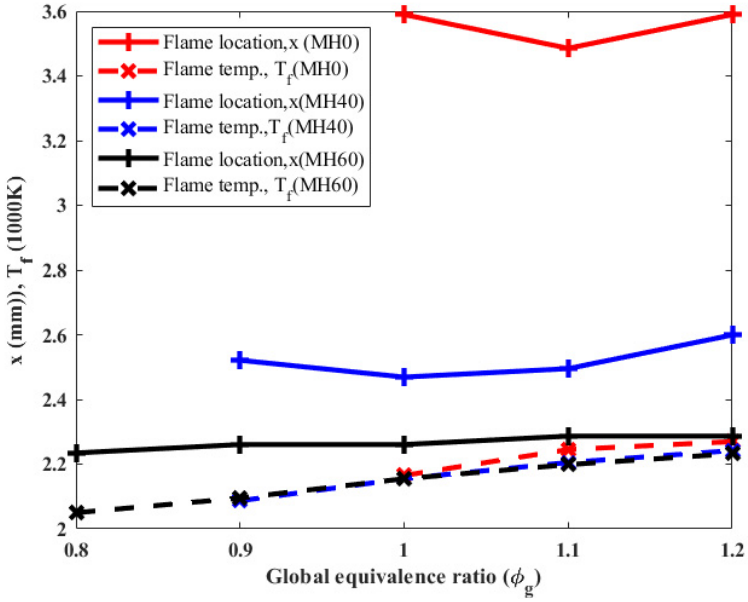

Figure 12. Variation in flame location and flame temperature at a global equivalence ratio (0.8, 1.0 and 1.2) for fuel compositions MH0, MH40, and MH60, while keeping air velocity constant (2 m/s).

Figure 13 demonstrates the variation in flame location and flame temperature as the global equivalence ratio varied from lean to rich conditions (0.8 to 1.2) for fuel compositions MH0, MH40, and MH60. For Φ_g = 1.0, MH0 exhibited a stable flame at a distance of about 2.3 mm downstream of the combustor inlet; this distance was reduced to about 2.25 mm for MH40. This distance was further reduced to about 2.2 mm for MH60. It can also be seen that for each fuel composition, flame location was slightly elevated in fuel-rich conditions. Additionally, flame temperature had the highest value (2100 K) for MH0 (at Φ_g = 1.2), which dropped with the addition of hydrogen. Moreover, the flame temperature range continuously decreased with addition of hydrogen [MH0—2070 K to 2080 K (Φ_g = 1.0–1.2); MH40—1850 K to 1950 K (Φ_g = 1.0–1.2); and MH60–1640 K to 1930 K (Φ_g = 0.8–1.2)].

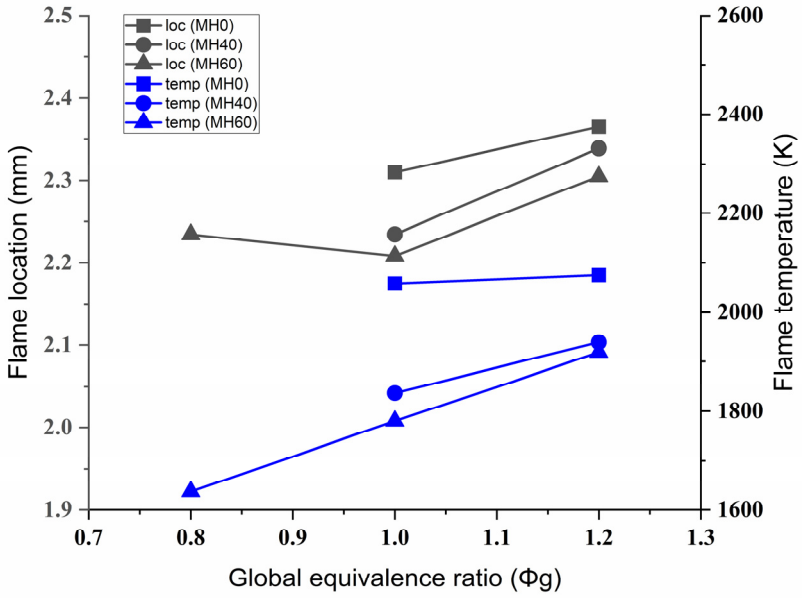

Figure 13. Variation in flame location and flame temperature at different global equivalence ratios (0.8, 1.0 and 1.2) for fuel compositions MH0, MH40, and MH60 at an inlet velocity of V_{fuel} = 0.1 m/s.

The flame stabilization of MH0 and MH60 at different global equivalence ratios (MH0: Φ_g = 1.0, 1.2 and MH60: Φ_g = 0.8,1.0 and 1.2) at an inlet velocity of V_{fuel} = 0.1 m/s is depicted in Figure 14; this was achieved by plotting the heat release rate along with the temperature profile. It is evident that the flame becomes weaker and the flame temperature also decreases with the addition of hydrogen to the fuel. The flame is anchored to the splitter at all equivalence ratios for MH60, whereas for MH0, it is stabilized further downstream of the combustor, as already observed in Figure 12. However, flame thickness was considerably reduced for MH60 compared to MH0, especially in lean conditions (Φ_g = 0.8). For MH0, when Φ_g was varied from 1.0 to 1.2 (going from stoichiometric to fuel-rich conditions), the flame height slightly increased, and the flame became more slanted downstream due to the reduced air flow compared to fuel flow. For MH60, a weaker flame was observed at Φ_g = 0.8, and as Φ_g was varied from 0.8 to 1.2 (going from lean to fuel-rich conditions), the flame height slightly increased and the flame shifted towards the air inlet due to the reduced air flow. Furthermore, at all equivalence ratios, the flame was located slightly towards the air inlet, where the mixing and reaction occurred due to the higher laminar burning velocity of hydrogen.

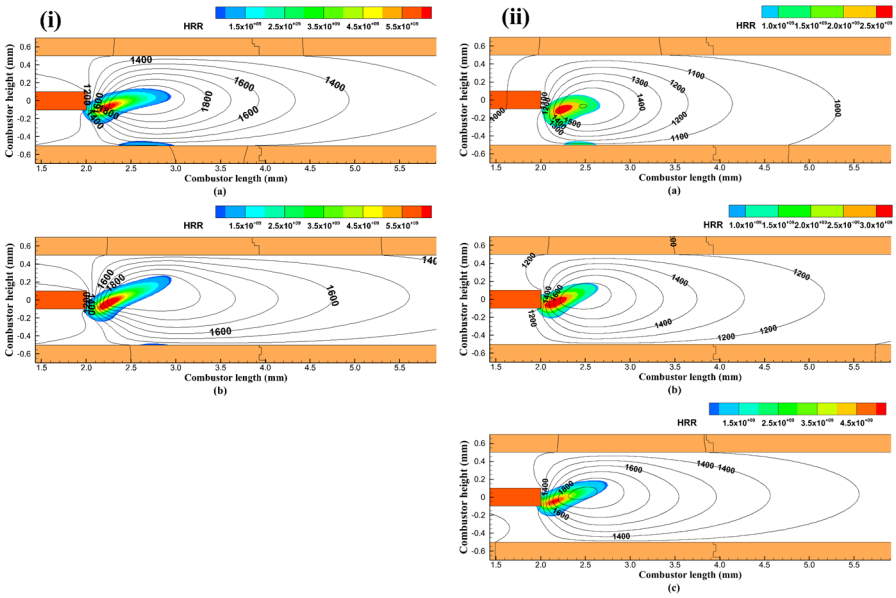

Figure 14. Heat release rate and temperature profile of (**i**) MH0 ((**a**) Φ_g = 1.2 (**b**) Φ_g = 1.0) and (**ii**) MH60: (**a**) Φ_g = 1.2; (**b**) Φ_g = 1.0; (**c**) Φ_g = 0.8 at an inlet velocity of V_{fuel} = 0.1 m/s.

Figure 15 shows the variation in combustor efficiency and combustion efficiency for different fuel compositions at global equivalence ratios of 0.8, 1.0 and 1.2. The trend in both combustor efficiency and combustion efficiency demonstrated a consistent decrease as the fuel inlet condition became richer. This trend confirms the general phenomenon wherein lean fuels burn completely, while incomplete combustion occurs for richer mixtures due to an excess of fuel beyond the stoichiometric ratio. Additionally, it is worth noting that for rich mixtures, the combustion efficiency was higher for MH60 compared to that for MH0 and MH40. The combustor efficiency (10–50%) was relatively low compared to the combustion efficiency (80–100%), as heat loss through the combustor walls was greater. Due to the complete combustion of the lean mixture, MH60 exhibited the maximum value for both combustion efficiency (100%) and combustor efficiency (44%) at Φ_g = 0.8, and then reduced as the mixture became rich. At a stoichiometric air–fuel ratio (Φ_g = 1.0), pure methane exhibited the highest values of 99% and 45% for combustion efficiency and combustor efficiency, respectively. As the authors look forward to the application of a thermo-electric generator module for generating power from micro-combustors, the heat of flue gases will be utilized, and heat transfer to the walls will be considered heat

loss. So, from the authors' perspective, the expression of combustion efficiency is more relevant. The expression of combustor efficiency is beneficial for thermo-photovoltaic power generation from micro-combustors, where wall temperature is predominant (rather than flue gas temperature).

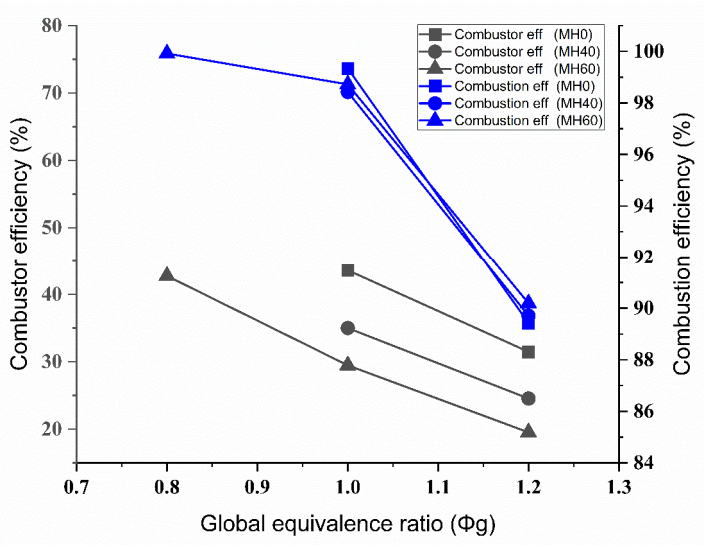

Figure 15. Variation in the combustion efficiency of different fuel combinations (MH0, MH40 and MH60) at different global equivalence ratios (Φ_g) ranging from 0.8 to 1.2.

3.3. Heat Recirculation Analysis

All the phenomena described in previous section were rationalized by performing a heat recirculation analysis in the combustor walls. As heat transfer through walls mostly relies on conduction, it was calculated with numerical results using Fourier's law:

$$q = k \frac{\partial T}{\partial x} \tag{9}$$

where 'k' was calculated using the law of ideal gas mixing. 'q' was considered positive when heat transfer occurred from wall to mixture and considered negative in both the cases when heat was transferred from mixture to wall and from the wall to surroundings, as shown in Figure 16. Heat transfer, Q (watts) was calculated by integrating the local heat flux, q (W/m^2), over the respective surface area (m^2). Here, with the combustor being a planar one (with unit width), heat flux (Q) was represented in W/m.

Q_1 = Heat flux from the flame to combustor wall (heat of combustion)
Q_2 = Heat flux through the combustor wall (heat conduction)
Q_3 = Heat flux from the combustor wall to surroundings (heat loss, Q_{loss})
Q_4 = Heat flux from the combustor wall to the mixture (heat recirculation, Q_{re})

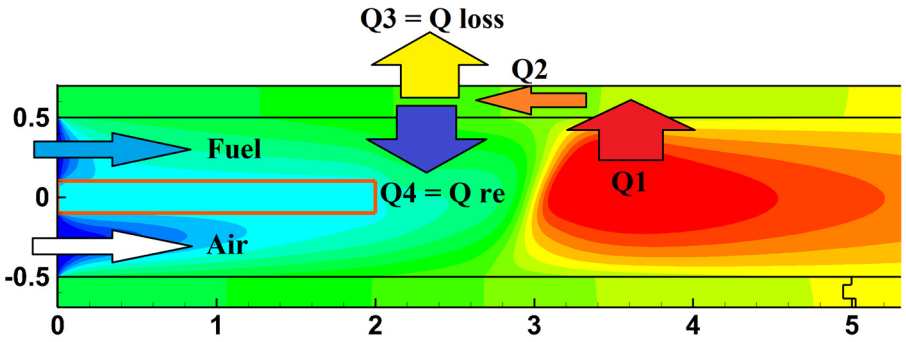

Figure 16. Local heat flux in the combustor wall.

Figure 15 demonstrates the methodology of heat recirculation analysis.

Table 2 displays the values of Q_{re} and Q_{loss} and the Q_{re}/Q_{loss} ratio as well as their trend for MH0. All these quantities were found to exhibit a monotonic variation with inlet velocity. Gao et al. [43] explained the effect of heat recirculation on methane–air flames.

Table 2. Tabulation of heat recirculation and heat loss for MH0 at different inlet velocities.

V_{air}	Q_{re}	Q_{loss}	Q_{total}	% Q_{re}	% Q_{loss}	Q_{re}/Q_{loss}
m/s	W/m	W/m	W/m	%	%	
1	243	371	614	39.55	60.45	0.65
1.5	438	448	886	49.44	50.56	0.98
2	489	478	968	55.55	49.45	1.02

Table 2 shows that heat recirculation was very low compared to heat loss from the wall at an inlet velocity of 1 m/s, which resulted in a lower outer wall temperature, as already observed in Figure 5(ii). As the unburnt gas temperature was very low, flame thickness as well as flame temperature were found to be low, although the flame was anchored at the tip of splitter. When the inlet velocity was increased to 1.5 m/s, there was an almost equal balance between heat recirculation and heat loss. Consequently, there was an enhancement in both flame thickness and flame temperature. However, this improvement led to the flame being lifted off the splitter, as depicted in Figures 4 and 5(ii,iii). When the velocity was further increased to 2 m/s, the ratio (Q_{re}/Q_{loss}) was found exceed unity (Figure 4(i)), and therefore V_{air} = 2 m/s can be considered the critical velocity for pure methane because the flame was completely lifted off and on the verge of blow-out. Although the flame was lifted off the splitter and the flame temperature remained the same, the outer wall temperature and the flame dimensions were found to be improved a lot, as seen in Figures 4 and 5(ii,iii).

Table 3 depicts the values of Q_{re} and Q_{loss} and Q_{re}/Q_{loss} ratio for the fuel composition MH60. Heat recirculation was found to follow a monotonic trend with inlet velocity. As seen in the case of MH0, when heat recirculation was very low (from Table 2) at an inlet velocity of 1 m/s, parameters like flame thickness, flame temperature, and outer wall temperature were observed to be minimal, as shown in Figure 7(ii) and Figure 10. As the velocity increased, heat recirculation also increased; consequently, the flame dimensions were improved, as shown in Figure 7(ii). It is also to be noted that the maximum outer wall temperature was observed at a 2.5 m/s inlet velocity, after which it was slightly reduced at higher velocity, as seen in Figure 10, because of the reduction in flame temperature (Figure 10(ii)). An inlet velocity value of 3 m/s was considered the critical velocity for the current fuel composition because the ratio of heat recirculation to heat loss just exceeded unity (Figure 7(ii)), where the flame started lifting off. In terms of flame location and flame temperature, an inlet velocity of 2 m/s was recommended as the critical velocity beyond which the flame was lifted off considerably and eventually blew out of the combustor.

Table 3. Tabulation of heat recirculation and heat loss with MH60 at different air velocities.

V_{air}	Q_{re}	Q_{loss}	Q_{total}	% Q_{re}	% Q_{loss}	Q_{re}/Q_{loss}
m/s	W/m	W/m	W/m	%	%	
1	291	474	765	38.03	61.97	0.61
1.5	412	495	907	45.46	54.54	0.83
2	505	517	1022	49.40	50.60	0.98
2.5	561	533	1094	51.27	48.73	1.05
3	570	518	1088	52.36	47.64	1.10

Table 4 tabulates the values of Q_{re} and Q_{loss} and the Q_{re}/Q_{loss} ratio for the fuel composition MH40. The selected composition was chosen as an intermediary to observe the progression of previously discussed parameter changes. Table 4 illustrates that heat recirculation followed a consistent, gradual increase, similar to the patterns observed in the other cases. Notably, at an inlet velocity of 2 m/s, this velocity can be deemed critical concerning heat recirculation. This is evidenced by the ratio of heat recirculation to heat loss surpassing unity, initiating the flame's tendency to lift off.

Table 4. Tabulation of heat recirculation and heat loss with MH40 at different air velocities.

V_{air}	Q_{re}	Q_{loss}	Q_{total}	% Q_{re}	% Q_{loss}	Q_{re}/Q_{loss}
m/s	W/m	W/m	W/m	%	%	
1	261	421	683	38.30	61.70	0.62
1.5	401	476	877	45.68	54.32	0.84
2	498	505	1003	49.65	50.35	0.99
2.5	542	524	1066	50.88	49.12	1.04
3	547	528	1075	50.89	49.11	1.04

The values of the Q_{re}/Q_{loss} ratio at different inlet velocities for MH0, MH40, and MH60 are plotted in Figure 17. This gives us a clear idea of the critical inlet velocity when the flame starts lifting off. Considering the present combustor, for fuels MH0, MH40, and MH60 the critical values of inlet velocity were 2 m/s, 2.5 m/s, and 2.5 m/s, respectively.

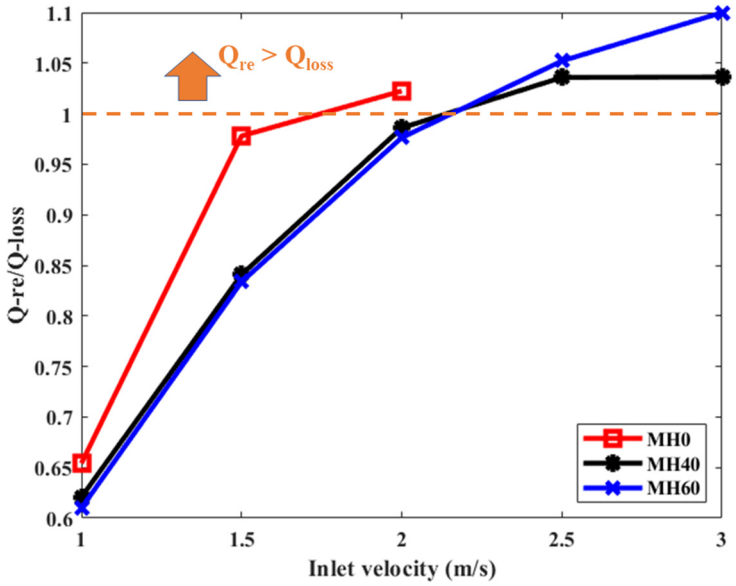

Figure 17. The ratio of Q-re to Q-loss of MH0, MH40, and MH60 at different inlet velocities.

4. Conclusions

This investigation focused on the non-premixed combustion characteristics of methane–hydrogen blends in a planar micro-combustor equipped with a splitter. The primary findings regarding the impact of hydrogen blending, inlet velocity, and global equivalence ratio on flame location, flame temperature, combustion efficiency, and outer wall temperature are outlined below.

1. The stability limit witnessed a significant increase of 50% with the addition of hydrogen, i.e., extending from 1–2 m/s for MH0 to 1–3 m/s for MH40 and MH60 at a stoichiometric air–fuel ratio (Φ_g = 1). This increased stability limit enabled the combustor to be operated for a wide range of velocities without extinguishing the flame.

2. The heat recirculation analysis of the combustor wall revealed a monotonic increase in the ratio of Q_{re} to Q_{loss} with increasing inlet velocity for all compositions. Moreover, as more heat was recirculated from the wall into unburnt gas compared to the heat loss from the wall to its surroundings ($Q_{re} > Q_{loss}$), the flame started lifting off, which can be used as a salient criterion of the diffusion of flames for determining occurrence of the lift-off phenomenon. The lift-off phenomenon affects the flame structure as well as wall temperature distribution, which subsequently affects the performance and operational range of the combustor.

3. From the study of the effect of hydrogen blending from MH0, MH40, and MH60 at an inlet velocity of 2 m/s and a global equivalence ratio (Φ_g) of unity, the flame location showed significant enhancement, reducing from 3.6 mm (MH0) to 2.2 mm (MH60). Additionally, there was a significant increase of 100 K in the outer wall temperature for MH60 compared to MH0. As more hydrogen was added to the fuel, the flame was stabilized further upstream of the combustor, which established the possibility of applying higher inlet velocity, which ultimately increased the operational range of the combustor. This increase in outer wall temperature will be advantageous for power generation using thermo-photovoltaic cells.

4. The effect of the global equivalence ratio can be studied either by varying inlet fuel velocity and keeping inlet air velocity constant (or vice versa). To understand the difference in both, simulations were initially performed by varying the inlet fuel velocity and keeping the inlet air velocity constant (2 m/s) in order to produce lean and rich conditions (Φ_g = 0.8–1.2) for the fuel compositions MH0, MH40, and MH60; then, the fuel inlet velocity was kept constant (V_{fuel} = 0.1 m/s) and the air velocity was varied to achieve the desired global equivalence ratios. Although the trend in the results of both the simulation setups remained the same with a difference in the magnitudes of both flame location and flame temperature, the latter results are more accurate as the results became comparable among different fuel compositions (MH0, MH40, and MH60) without much variation in firing rate. While the flames failed to stabilize for lean air–fuel ratios of MH0 and MH40, a stable flame was achieved for MH60 at Φ_g = 0.9 and 0.8. MH60 in lean conditions ensured a cleaner combustion (without emission) by providing a stable flame by complete combustion. Flame location and flame temperature showed a consistent reduction with the increase in the amount of hydrogen in the fuel. Flame temperature increased as the global equivalence ratio increased for each composition. At Φ_g = 1.0, flame location decreased from 2.33 mm (MH0) to 2.2 mm (MH60), and flame temperature decreased from 2070 K(MH0) to 1800 K(MH60).

Moreover, combustor efficiency and combustion efficiency decreased as the global equivalence ratio increased for each composition. Due to complete combustion of the lean mixture, MH60 exhibited the maximum value for both combustion efficiency (100%) and combustor efficiency (44%) at Φ_g = 0.8 and then reduced as the mixture became rich. At a stoichiometric air–fuel ratio (Φ_g = 1.0), pure methane exhibited the highest values of 99% and 45% for combustion efficiency and combustor efficiency, respectively.

On the whole, the addition of hydrogen to the blend extended the stability thresholds for both the inlet velocity and global equivalence ratio of methane. The enhanced outer wall temperature suggests potential applications in micro-power generation utilizing thermo-photovoltaic cells. Moreover, potential improvements in stability limits can be explored further through minor modifications to the shape and dimensions of the splitter.

Author Contributions: Conceptualization, R.K.V. and P.S.; methodology, R.K.V. and S.S.; software, R.K.V., S.S. and P.S.; validation, R.K.V. and S.S.; formal analysis, A.B.S.A.; investigation, S.S.; resources, R.K.V.; data curation, S.S.; writing—original draft preparation, S.S.; writing—review and editing, P.S. and A.B.S.A.; supervision, R.K.V.; project administration, R.K.V.; funding acquisition, R.K.V. All authors have read and agreed to the published version of the manuscript.

Funding: The authors would like to thank the Science and Engineering Research Board, DST, India, for their support through grant number CRG/2021/003079 under the Core Research Grant scheme.

Data Availability Statement: Data are contained within the article.

Conflicts of Interest: The authors declare no conflicts of interest.

Nomenclature

FREI	Flame with repetitive extinction and ignition
MEMS	Micro-electro-mechanical systems
Phi	Equivalence ratio
LBV	Laminar burning velocity, m/s
ESR	Extinction strain rate
TPV	Thermo-photovoltaic
W_0	Combustor wall thickness, mm
W_1	Splitter thickness, mm
H_0	Combustor height, mm
H_1	Air inlet port height, mm
L_0	Combustor length, mm
L_1	Splitter length, mm
K_n	Knudsen number
Re	Reynolds number
$\boldsymbol{\rho}$	Density of fluid, kg/m^3
η_c	Combustion efficiency, %
$\boldsymbol{u}$	Velocity component, m/s
P	Gas pressure, Pa
k_f	Thermal conductivity of fluid, W/m-K
h_j	Enthalpy of *jth* species, J/kg
MH0	Fuel composition with 100% CH_4 - 0% H_2 by volume
MH40	Fuel composition with 60% CH_4 - 40% H_2 by volume
MH60	Fuel composition with 40% CH_4 - 60% H_2 by volume
h	Natural heat transfer coefficient, W/mˆ2-K
T_w	Outer wall temperature, K
T_∞	Ambient temperature, K
FVM	Finite volume method
Φ_g	Global equivalence ratio
V_{air}	Inlet air velocity, m/s

References

1. Fernandez-Pello, A.C. Micropower Generation Using Combustion: Issues and Approaches. *Proc. Combust. Inst.* **2002**, *29*, 883–899. [CrossRef]
2. Jiang, L.Q.; Zhao, D.Q.; Guo, C.M.; Wang, X.H. Experimental Study of a Plat-Flame Micro Combustor Burning DME for Thermoelectric Power Generation. *Energy Convers. Manag.* **2011**, *52*, 596–602. [CrossRef]
3. Yang, W.M.; Chou, S.K.; Li, J. Microthermophotovoltaic Power Generator with High Power Density. *Appl. Therm. Eng.* **2009**, *29*, 3144–3148. [CrossRef]
4. Li, L.; Yuan, Z.; Xiang, Y.; Fan, A. Numerical Investigation on Mixing Performance and Diffusion Combustion Characteristics of H_2 and Air in Planar Micro-Combustor. *Int. J. Hydrogen Energy* **2018**, *43*, 12491–12498. [CrossRef]
5. Pan, J.; Zhang, R.; Lu, Q.; Zha, Z.; Bani, S. Experimental Study on Premixed Methane-Air Catalytic Combustion in Rectangular Micro Channel. *Appl. Therm. Eng.* **2017**, *117*, 1–7. [CrossRef]
6. Zarvandi, J.; Tabejamaat, S.; Baigmohammadi, M. Numerical Study of the Effects of Heat Transfer Methods on $CH_4/(CH_4 + H_2)$-AIR Pre-Mixed Flames in a Micro-Stepped Tube. *Energy* **2012**, *44*, 396–409. [CrossRef]
7. Gao, W.; Yan, Y.; Huang, L.; Shen, K.; He, Z.; Gao, B. Numerical Comparison of Premixed H_2/Air Combustion Characteristic of Three Types of Micro Cavity-Combustors with Guide Vanes, Bluff Body, Guide Vanes and Bluff Body Respectively. *Int. J. Hydrogen Energy* **2021**, *46*, 24382–24394. [CrossRef]
8. Li, J.; Li, Q.; Wang, Y.; Guo, Z.; Liu, X. Fundamental Flame Characteristics of Premixed H_2-Air Combustion in a Planar Porous Micro-Combustor. *Chem. Eng. J.* **2016**, *283*, 1187–1196. [CrossRef]
9. Yang, X.; He, Z.; Zhao, L.; Dong, S.; Tan, H. Effect of Channel Diameter on the Combustion and Thermal Behavior of a Hydrogen/Air Premixed Flame in a Swirl Micro-Combustor. *Energies* **2019**, *12*, 3821. [CrossRef]

10. Bagheri, G.; Hosseini, S.E.; Wahid, M.A. Effects of Bluff Body Shape on the Flame Stability in Premixed Micro-Combustion of Hydrogen-Air Mixture. *Appl. Therm. Eng.* **2014**, *67*, 266–272. [CrossRef]
11. Tang, A.; Deng, J.; Xu, Y.; Pan, J.; Cai, T. Experimental and Numerical Study of Premixed Propane/Air Combustion in the Micro-Planar Combustor with a Cross-Plate Insert. *Appl. Therm. Eng.* **2018**, *136*, 177–184. [CrossRef]
12. Cai, T.; Zhao, D.; Karimi, N. Optimizing Thermal Performance and Exergy Efficiency in Hydrogen-Fueled Meso-Combustors by Applying a Bluff-Body. *J. Clean. Prod.* **2021**, *311*, 127573. [CrossRef]
13. Cai, T.; Zhao, D.; Ji, L.; Agarwal, A.K. Removal and Mechanism Analysis of NO_x Emissions in Carbon-Free Ammonia Combustion Systems with a Secondary Fuel Injection. *Fuel* **2023**, *344*, 128088. [CrossRef]
14. Singh, A.P.; Kishore, V.R.; Yoon, Y.; Minaev, S.; Kumar, S. Effect of Wall Thermal Boundary Conditions on Flame Dynamics of CH_4-Air and H_2-Air Mixtures in Straight Microtubes. *Combust. Sci. Technol.* **2017**, *189*, 150–168. [CrossRef]
15. Lamioni, R.; Bronzoni, C.; Folli, M.; Tognotti, L.; Galletti, C. Effect of Slit Pattern on the Structure of Premixed Flames Issuing from Perforated Burners in Domestic Condensing Boilers. *Combust. Theory Model.* **2023**, *27*, 218–243. [CrossRef]
16. Ma, L.; Fang, Q.; Zhang, C.; Chen, G. A Novel Swiss-Roll Micro-Combustor with Double Combustion Chambers: A Numerical Investigation on Effect of Solid Material on Premixed CH_4/Air Flame Blow-off Limit. *Int. J. Hydrogen Energy* **2021**, *46*, 16116–16126. [CrossRef]
17. Sankar, V.; Sudarsanan, S.; Mukhopadhyay, S.; Selvaraj, P.; Balakrishnan, A.; Velamati, R.K. Towards the Development of Miniature Scale Liquid Fuel Combustors for Power Generation Application—A Review. *Energies* **2023**, *16*, 4035. [CrossRef]
18. Cai, S.; Yang, W.; Ding, Y.; Zeng, Q.; Wan, J. Hydrogen-Air Premixed Combustion in a Novel Micro Disc-Burner with an Annular Step. *Fuel* **2022**, *313*, 123015. [CrossRef]
19. Cai, T.; Tang, A.; Zhao, D.; Zhou, C.; Huang, Q. Flame Dynamics and Stability of Premixed Methane/Air in Micro-Planar Quartz Combustors. *Energy* **2020**, *193*, 116767. [CrossRef]
20. Singh, S.; Veetil, J.E.; Kumbhakarna, N.; Velamati, R.K.; Kumar, S. Flame Dynamics of Premixed CH_4/H_2/Air Flames in a Microchannel with a Wall Temperature Gradient. *Combust. Theory Model.* **2022**, *26*, 989–1013. [CrossRef]
21. Peng, Q.; Ye, J.; Tu, Y.; Yang, W.; Jiaqiang, E.; Kang, Z.; Fu, G. Experimental and Numerical Investigation on Premixed H_2/C_3H_8/Air Combustion and Thermal Performance in a Burner with Partially Filled Porous Media. *Fuel* **2022**, *328*, 125227. [CrossRef]
22. Liu, Y.; Zhang, J.; Fan, A.; Wan, J.; Yao, H.; Liu, W. Numerical Investigation of CH_4/O_2 Mixing in Y-Shaped Mesoscale Combustors with/without Porous Media. *Chem. Eng. Process. Process Intensif.* **2014**, *79*, 7–13. [CrossRef]
23. Ning, D.; Liu, Y.; Xiang, Y.; Fan, A. Experimental Investigation on Non-Premixed Methane/Air Combustion in Y-Shaped Meso-Scale Combustors with/without Fibrous Porous Media. *Energy Convers. Manag.* **2017**, *138*, 22–29. [CrossRef]
24. Muraleedharan, A.; Veetil, J.E.; Mohammad, A.; Kumar, S.; Velamati, R.K. Effect of Burner Wall Material on Microjet Hydrogen Diffusion Flames near Extinction: A Numerical Study. *Energies* **2021**, *14*, 8266. [CrossRef]
25. Xiang, Y.; Yuan, Z.; Wang, S.; Fan, A. Effects of Flow Rate and Fuel/Air Ratio on Propagation Behaviors of Diffusion H_2/Air Flames in a Micro-Combustor. *Energy* **2019**, *179*, 315–322. [CrossRef]
26. Li, L.; Fan, A. A Numerical Study on Non-Premixed H_2/Air Flame Stability in a Micro-Combustor with a Slotted Bluff-Body. *Int. J. Hydrogen Energy* **2021**, *46*, 2658–2666. [CrossRef]
27. He, Z.; Yan, Y.; Fang, R.; Ou, Z.; Zhang, Z.; Yang, Z.; Zhang, Z. Numerical Investigation of a Novel Micro Combustor with a Central and Bilateral Slotted Blunt Body. *Int. J. Hydrogen Energy* **2021**, *46*, 23564–23579. [CrossRef]
28. Yang, X.; Zhao, L.; He, Z.; Dong, S.; Tan, H. Comparative Study of Combustion and Thermal Performance in a Swirling Micro Combustor under Premixed and Non-Premixed Modes. *Appl. Therm. Eng.* **2019**, *160*, 114110. [CrossRef]
29. Wan, J.; Zhao, H. Laminar Non-Premixed Flame Patterns in Compact Micro Disc-Combustor with Annular Step and Radial Preheated Channel. *Combust. Flame* **2021**, *227*, 465–480. [CrossRef]
30. Zhou, C.; Tang, A.; Cai, T.; Zhao, D.; Huang, Q. Numerical Study on Flame Shape Transition and Structure Characteristic of Premixed CH_4/H_2-Air in the Micro-Planar Combustor. *Chem. Eng. Process. Process Intensif.* **2021**, *166*, 108460. [CrossRef]
31. Balaji, R.K.; Rajan, K.P.; Ragula, U.B.R. Modeling & Optimization of Renewable Hydrogen Production from Biomass via Anaerobic Digestion & Dry Reformation. *Int. J. Hydrogen Energy* **2020**, *45*, 18226–18240. [CrossRef]
32. Hou, B.; Fan, A. A Numerical Study on the Combustion Limits of Mesoscale Methane Jet Flames with Hydrogen Addition. *Int. J. Hydrogen Energy* **2022**, *47*, 30639–30652. [CrossRef]
33. Guo, L.; Zhai, M.; Xu, S.; Shen, Q.; Dong, P.; Bai, X.S. Flame Characteristics of Methane/Air with Hydrogen Addition in the Micro Confined Combustion Space. *Int. J. Hydrogen Energy* **2022**, *47*, 19319–19337. [CrossRef]
34. Wang, Y.; Wang, J.; Pan, J.; Lu, Q.; Li, F.; Quaye, E.K. Effects of Hydrogen-Addition on the FREI Dynamics of Methane/Oxygen Mixture in Meso-Scale Reactor. *Fuel* **2022**, *311*, 122506. [CrossRef]
35. Raissi, H. The Effects of Added Hydrogen to Premixed Methane and Air in an MEMS Channel. *J. Heat Mass Transf. Res.* **2020**, *7*, 55–62. [CrossRef]
36. Eckart, S.; Rong, F.Z.; Hasse, C.; Krause, H.; Scholtissek, A. Combined Experimental and Numerical Study on the Extinction Limits of Non-Premixed H_2/CH_4 Counterflow Flames with Varying Oxidizer Composition. *Int. J. Hydrogen Energy* **2023**, *48*, 14068–14078. [CrossRef]

37. Rajamanickam, K.; Lefebvre, F.; Gobin, C.; Godard, G.; Lacour, C.; Lecordier, B.; Cessou, A.; Honoré, D. Effect of H_2 Addition on the Local Extinction, Flame Structure, and Flow Field Hydrodynamics in Non-Premixed Bluff Body Stabilized Flames. *Phys. Fluids* **2023**, *35*, 047110. [CrossRef]
38. Shin, C.; Nam, H.T.; Lee, S. Effect of Hydrogen Addition on Flame Stability and Structure for Low Heating Value Coaxial Nonpremixed Flames. *Combust. Sci. Technol.* **2023**, *195*, 2933–2951. [CrossRef]
39. Wei, D.; Peng, Q.; Wang, H.; Tian, X.; Xiao, H.; Liu, H.; Fu, G. Experimental Investigation of Blended H_2/CH_4 Combustion in Combustors with Block for Micro-Thermophotovoltaic. *Fuel* **2024**, *357*, 129869. [CrossRef]
40. GRI-MECH 3.0. Available online: http://combustion.berkeley.edu/gri-mech/ (accessed on 8 September 2023).
41. ANSYS. *Ansys®Fluent, 2023-R1*; Help System; ANSYS Inc.: Ann Arbor, MI, USA, 2023.
42. Jiaqiang, E.; Peng, Q.; Zhao, X.; Zuo, W.; Zhang, Z.; Pham, M. Numerical Investigation on the Combustion Characteristics of Non-Premixed Hydrogen-Air in a Novel Micro-Combustor. *Appl. Therm. Eng.* **2017**, *110*, 665–677. [CrossRef]
43. Gao, J.; Hossain, A.; Matsuoka, T.; Nakamura, Y. A Numerical Study on Heat-Recirculation Assisted Combustion for Small Scale Jet Diffusion Flames at near-Extinction Condition. *Combust. Flame* **2017**, *178*, 182–194. [CrossRef]